Geophysical Research Letters

RESEARCH LETTER
10.1029/2023GL106606

Hybrid Simulation of Magnetosheath Jet-Driven Bow Waves

Junyi Ren[1,2], Quanming Lu[1,2,3], Xinliang Gao[1,2,3], Michael Gedalin[4], Huixuan Qiu[5], Desheng Han[5], and Rongsheng Wang[1,2,3]

[1]CAS Key Laboratory of Geospace Environment, School of Earth and Space Sciences, University of Science and Technology of China, Hefei, China, [2]CAS Center for Excellence in Comparative Planetology, Hefei, China, [3]Collaborative Innovation Center of Astronautical Science and Technology, Harbin, China, [4]Department of Physics, Ben-Gurion University of the Negev, Beer-Sheva, Israel, [5]State Key Laboratory of Marine Geology, School of Ocean and Earth Science, Tongji University, Shanghai, China

Key Points:

- We study the formation and evolution of jet-driven bow waves with the two-dimensional hybrid model for the first time
- Plasma piles up at the ramp of compressed magnetic field, causing separated peaks of density and magnetic field at the bow wave
- The magnetic field structure acts as an obstacle to decelerate jet, causing the pile up of jet ions at the leading edge

Supporting Information:

Supporting Information may be found in the online version of this article.

Correspondence to:

Q. Lu and X. Gao,
qmlu@ustc.edu.cn;
gaox1@ustc.edu.cn

Citation:

Ren, J., Lu, Q., Gao, X., Gedalin, M., Qiu, H., Han, D., & Wang, R. (2024). Hybrid simulation of magnetosheath jet-driven bow waves. *Geophysical Research Letters*, *51*, e2023GL106606. https://doi.org/10.1029/2023GL106606

Received 29 SEP 2023
Accepted 17 DEC 2023

Abstract High-speed jets (HSJs) are commonly observed in the Earth's magnetosheath. The HSJs can drive shock-like bow waves when compressing the ambient plasma, which are important for the HSJ's evolution and the energization of charged particles. Here we present the first two-dimensional hybrid simulation of the formation and evolution of jet-driven bow waves. The simulated bow waves exhibit localized enhanced magnetic field and ion density, with their peaks separated by the order of ion inertial length. The bow waves are formed when a super-magnetosonic HSJ encounters a magnetic structure with the magnetic field nearly perpendicular to the HSJ's velocity. The magnetic field structure acts as an obstacle to deflect and decelerate the jet, causing the pile up of ions on the jet side and the compression of the magnetic structure on the downstream side. Our study explains the observed properties of bow waves, and helps to better understand the evolution of HSJs.

Plain Language Summary When the solar wind interacts with the Earth's magnetic field, it creates a bow shock in front of the magnetosphere. The bow shock slows down and heats up the solar wind plasma, creating a turbulent area known as the magnetosheath. Sometimes, high-speed jets (HSJ), observed as high velocity and density pulses, are detected in the magnetosheath. The HSJs can transfer the solar wind plasma through the magnetosheath and potentially affect the near-Earth space where satellites orbit. Recent studies have found that the HSJs can drive shock-like bow waves at their front. The bow waves can accelerate and heat up plasma, similar to the primary shock wave, and they play an important role in the evolution of the HSJs. In this study, we present the first simulation result concerning the formation and evolution of the bow waves, which will help us to better understand the HSJs and the magnetosheath dynamics.

1. Introduction

High-speed jets (HSJs), characterized by localized large dynamic pressure, are commonly observed in the Earth's magnetosheath downstream of the quasi-parallel shock (Archer & Horbury, 2013; Hietala et al., 2009; Němeček et al., 1998, etc.). The spatial size of magnetosheath jets is about 1 R_E (where R_E is the Earth's radius), and their recurrence time is on the order of several minutes (Plaschke et al., 2013). Magnetosheath HSJs are attracting more and more attention because of their significant geospace effects. After impinging on the magnetopause, they can cause large amplitude boundary indentations, possibly triggering dayside magnetic reconnection (Hietala et al., 2009), exciting magnetopause surface waves or compressional waves in the magnetosphere (Plaschke et al., 2009), and resulting in dayside fast flow channels in the ionosphere (Hietala et al., 2012) and localized auroral brightening (Wang et al., 2018). Several mechanisms have been proposed to explain the formation of HSJs, such as the converging effect on the solar wind flow due to the rippled geometry of the shock front (Hao et al., 2016; Hietala et al., 2009), the interaction between foreshock compressive structures with the shock front (Karlsson et al., 2015; Raptis, Karlsson, Vaivads, Pollock, et al., 2022), or both (Ren et al., 2023).

HSJs in the magnetosheath are typically super-Alvénic and can be even super-magnetosonic, so it is natural for HSJs to drive shock-like bow waves when they compress the background plasma. Liu et al. (2019) observed such bow waves propagating downstream with sharp increases in the magnetic field and density. Hietala et al. (2009) reported a secondary shock that has similar properties but propagates upstream in the plasma rest frame. The bow waves are also found in a global hybrid simulation (Karimabadi et al., 2014). Liu, Hietala, Angelopoulos, Omelchenko, et al. (2020) conducted a statistical survey of the HSJ-driven bow waves with the THEMIS data, and

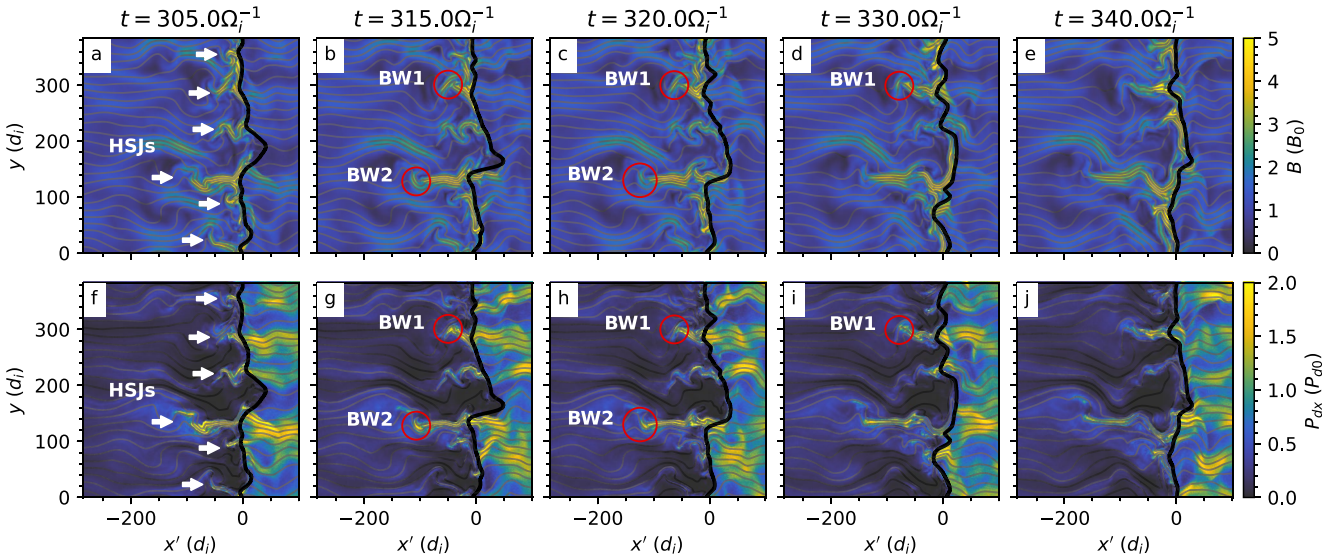

Figure 1. Evolution of the shock shown by (a–c) the total magnetic field B and (d–f) x component of the dynamic pressure P_{dx} in the shock frame. The bold black lines shows the location of the shock front, and the thin black lines represent the magnetic field lines projected in the x-y plane. Bow waves at $t = 320$ are marked by the red circles.

they showed about 13% of super-magnetosonic HSJs have bow waves at the leading edge. Both observations (Liu, Hietala, Angelopoulos, Omelchenko, et al., 2020; Liu, Hietala, Angelopoulos, Vainio, & Omelchenko, 2020) and simulations (Vuorinen et al., 2022) suggested that such bow waves can accelerate ions and electrons, which may further contribute to the parent shock acceleration. However, both the formation and evolution of bow waves driven by HSJs still remain unclear.

In this Letter, with the help of a two-dimensional (2-D) hybrid model, we reveal the time evolution of HSJ-driven bow waves downstream of a parallel shock, and well explain their formation and observed properties. This Letter is organized as follows. We describe the simulation model and setup in Section 2. The analysis of simulation results is presented in Section 3, and we conclude with a summary in Section 4 and discuss the implications of our results.

2. Simulation Model

This study utilizes a 2-D hybrid simulation code developed by Lu et al. (2006). In the simulation, the magnetic field is uniformly initialized with the value $\mathbf{B}_0 = B_0\hat{x}$ within the x-y simulation plane. The plasma is initialized with a uniform density N_0 and a velocity of $\mathbf{V}_0 = -6\ V_{A0}\hat{x}$, where $V_{A0} = B_0/\sqrt{\mu_0 m_p N_0}$ is the upstream Alfvén speed. The right x boundary of the simulation domain continuously injects plasma at the same velocity while allowing outgoing particles, while the left x boundary reflects particles, leading to the formation of the shock through the interaction between the reflected and incident plasma. Meanwhile, both y boundaries of the simulation domain are periodic. The simulation domain has dimensions of $1024 \times 384\ d_i^2$ and the grid resolution is $0.5\ d_i$ in the x and y directions, respectively, where d_i represents the upstream ion inertial length. Each grid cell is initialized with 100 macro-particles. The plasma beta is initialized as $\beta_p = \beta_e = 0.3$. The simulation time step is $\Delta t = 0.01\ \Omega_i^{-1}$ with $\Omega_i = eB_0/m_p$ being the upstream ion angular gyrofrequency.

3. Simulation Results

Figure 1 shows an overview of the parallel shock and its downstream, including the total magnetic field B and the x component of the dynamic pressure $P_{dx} = N_i(V_{ix} - V_{sh})^2$ at different times. For convenience, we present all the simulation results (Figures 1–4) in the shock frame and locate the shock front at approximately $x' = 0$. The shock reaches a fully developed state after $\sim 60\ \Omega_i^{-1}$ and propagates along the positive x direction at a nearly constant velocity of $V_{sh} \simeq 1.3\ V_{A0}$ in this case. The Alfvén Mach number is $M_A \simeq 7.3$ in the shock frame. Here the time interval from $305\ \Omega_i^{-1}$ to $340\ \Omega_i^{-1}$ is chosen without any preference but covers the entire evolution process of the HSJ-driven bow waves. At $t = 305\ \Omega_i^{-1}$, it is shown that there are six HSJs (denoted by the white arrows) newly formed in the nearby downstream, which are characterized by the strong enhancements of dynamic

pressure (Figure 1f). Those HSJs are caused by the interaction between the upstream compressive structures and the rippled shock front (Figure 1a), and the detailed generation process of the HSJs has been presented in Ren et al. (2023). We focus on the two strongest HSJs at around $y = 300\ d_i$ and $120\ d_i$, and they continue to grow in size until $\sim 320\ \Omega_i^{-1}$ (Figures 1c and 1h). Meanwhile, the shock-like bow waves BW1 and BW2 (marked by red circles) appear at the leading edges of the two HSJs and propagate deeper downstream along with the corresponding HSJ. Here, the bow waves are identified as sharp drops of the total magnetic field and ion density ahead of HSJs with super-magnetosonic ion velocity along the normal direction of the discontinuity, and the value changes should also satisfy the criterion described in Liu et al. (2019), Liu, Hietala, Angelopoulos, Omelchenko, et al. (2020): density and total magnetic field in the HSJ should be at least 0.2 times larger than the background plasma, and the velocity change between the HSJ and the background should be greater than 40% of the background speed. Subsequently, BW1 and BW2 begin to dissipate and disappear at about $340\ \Omega_i^{-1}$ (Figures 1e and 1j) and $330\ \Omega_i^{-1}$ (Figures 1e and 1j), respectively.

To clearly illustrate the detailed properties of BW1, Figure 2 provides an enlarged view of BW1 at $t = 320\ \Omega_i^{-1}$ (left column). As shown in Figure 2a, the shock-like bow wave is standing at the leading edge of the super-magnetosonic HSJ, where the jet interacts with the distorted magnetic field that is nearly perpendicular to the bulk velocity of the jet. At the bow wave, there are sharp increases in the magnetic field (Figure 2d) and density (Figure 2b), and a decrease in the bulk velocity (Figure 2c), which is consistent with the previous observations (Liu et al., 2019; Liu, Hietala, Angelopoulos, Omelchenko, et al., 2020). The right column displays the profiles of key parameters along the bow wave's normal direction (black dashed lines in Figures 2a–2d), where the shaded region represents the bow wave. In these figures, s is defined as the distance along the bow wave's normal direction, centered at the location where the gradient of ion density peaks. The fast-magnetosonic Mach number M_f of the HSJ can reach up to ~2.0 (Figure 2f), and the dominant velocity of the HSJ is the x component (Figure 2h). From the jet side to the downstream side, the bulk velocity decreases from $\sim 4.3\ V_{A0}$ to $\sim 1.5\ V_{A0}$ in the shock frame (Figure 2g), which is caused by the sudden braking of the jet. Although both magnetic field and density are rapidly enhanced as expected (Figures 2h and 2i), there exist two significant differences between them. First, the density reaches its maximum on the jet side of the bow wave, while the magnetic field peaks on the downstream side, with a spatial separation of $\sim 1.8\ d_i$. This phenomenon can also be found in satellite data (Liu et al., 2019; Liu, Hietala, Angelopoulos, Omelchenko, et al., 2020), but has been neglected. Second, the width of the density enhancement is estimated as 2.8 d_i with the Gaussian fitting, which is much narrower than that ($\sim 6.8\ d_i$) of the enhancement of the magnetic field.

To show the formation and evolution of the bow wave BW1, we plot the time evolution of the line profile along the bow wave's normal direction (purple dashed lines in Movie S1) between $t = 300$ and $335\ \Omega_i^{-1}$ in Figure 3. The $s = 0$ points at each time are defined as $\mathbf{X}_{\rm bw1} + \mathbf{V}_{\rm bw1}(t - 320)$, where $\mathbf{X}_{\rm bw1}$ and $\mathbf{V}_{\rm bw1}$ ($\simeq (-2.21, 0.53)\ V_{A0}$ in the shock frame) are the bow wave's position and velocity at $t = 320\ \Omega_i^{-1}$, respectively. At around $t = 310\ \Omega_i^{-1}$, the HSJ encounters the distorted magnetic field at the leading edge, whose dominant component is B_y, nearly perpendicular to the bulk velocity of the jet ($\theta_{Bn} > 60°$, Figure 3a). The velocity of the distorted magnetic field structure along the bow wave's normal is around $0.39\ V_{A0}$ in the bow wave frame when interacting with the HSJ, which is estimated by linear fitting the path of the magnetic field peak between $t = 310$ and $t = 320$ (black dotted line in Figure 3c). Here the "bow wave frame" is defined as the reference frame moving with a velocity of $\mathbf{V}_{\rm bw1}$ and is analogous to the rest normal incidence frame of the bow wave, as the bow wave's velocity hardly changes throughout its lifetime. Meanwhile, the bulk velocity at the center of the HSJ along the bow wave's normal is about $2\ V_{A0}$ in the same frame and the magnetosonic speed in the HSJ is about $1.8\ V_{A0}$. This means that the HSJ impacts the distorted magnetic field at a super-magnetosonic speed (also shown by dashed line encircled regions). As a result, the ion density begins to increase on the jet side due to the braking of the jet, while the magnetic field structure is compressed on the downstream side. The width of the magnetic field peak shrinks while its amplitude keeps growing till $320\ \Omega_i^{-1}$, and the bow wave with the localized enhancements of ion density and magnetic field is now formed. This demonstrates that the enhanced magnetic field acts as an obstacle, which deflects the jet and causes the pile up of ions on the jet side. After $320\ \Omega_i^{-1}$, the bulk velocity in the HSJ starts to decrease to around 3 V_{A0}, and the bow wave starts to dissipate with the density and magnetic field enhancements being weakened.

We also present the map of ion flow in the bow wave frame at $t = 320\ \Omega_i^{-1}$ to better understand the interaction between the jet and the magnetic obstacle. Figure 4 shows the total magnetic field B as well as the direction of the ion bulk velocity in the bow wave frame projected in the simulation plane. The bow wave (BW1) with the sharp enhancement of magnetic field is located in front of the jet, which deflects the ions on the jet side from the normal direction to the tangential direction. This will cause the sudden deceleration of the ions at the leading edge of the

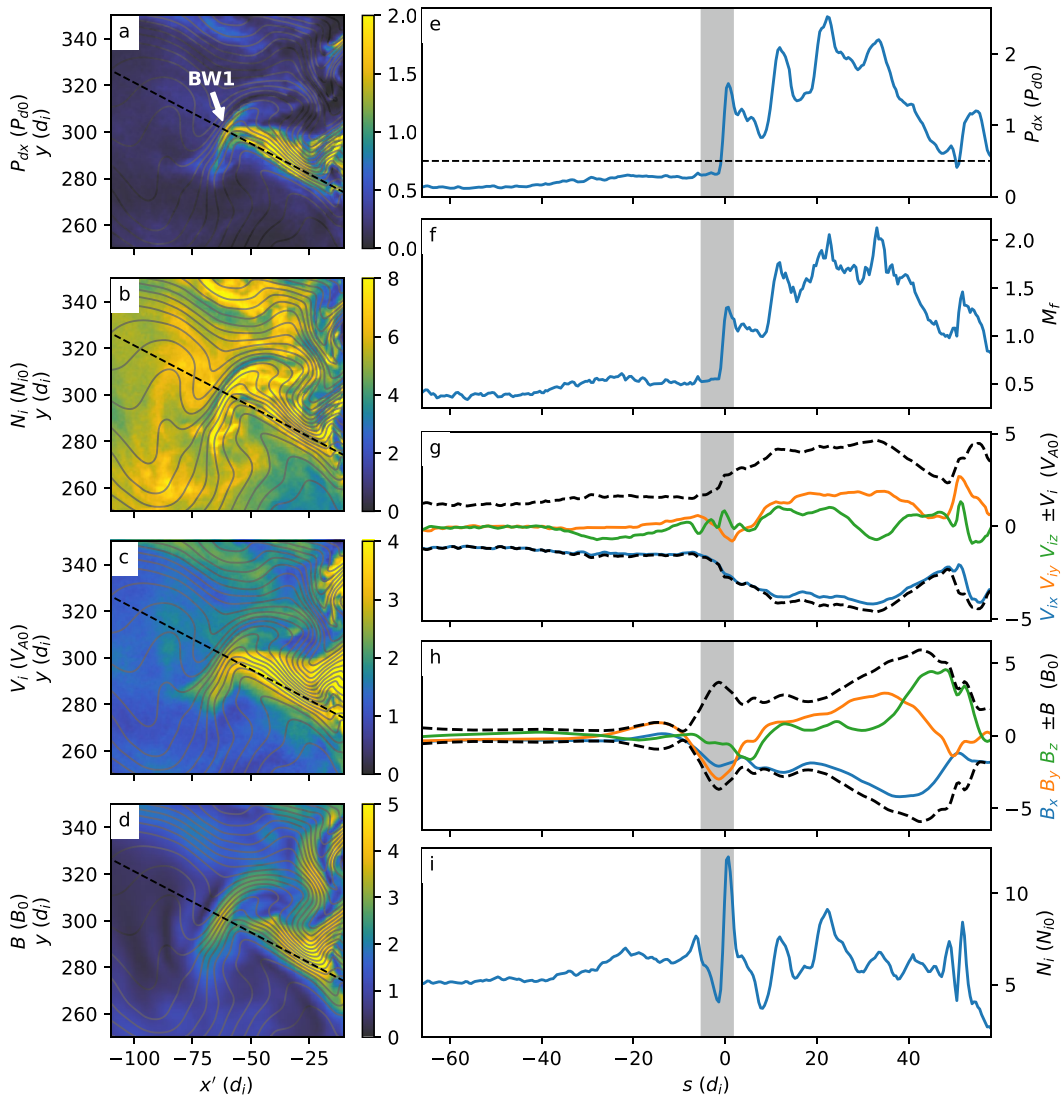

Figure 2. Panels (a–d) show the enlarged view of bow wave BW1 at $t = 320\ \Omega_i^{-1}$: (a) x component of the dynamic pressure P_{dx}, (b) ion density N_i, (c) ion velocity V_i, and (d) total magnetic field B. The solid black lines represent the magnetic field lines projected in the x-y plane. Panels (e–i) show the line profile along the dashed bow wave's normal direction (block lines in panels a–d). The plotted parameters are (e) the x component of the dynamic pressure P_{dx} where the horizontal black dashed line denotes 0.5 P_{d0}, (f) local fast-magnetosonic Mach number M_f, (g) ion velocityV_{ix} (blue), V_{ix} (orange), V_{ix} (green), and total value $\pm V_i$ (black, dashed), (h) Magnetic field B_x (blue), B_y (orange), B_z (green) and total strength $\pm B$ (black, dashed), and (i) ion density N_i. The shaded region represents the bow wave, and the s is the distance along the bow wave's normal centered at the ion density gradient peak.

jet, and then the significant drop of the normal velocity must result in the pile up of ions on the jet side, that is, the sharp enhancement of ion density. The flow direction differs from the expected behavior of a stationary shock because the bow wave is under rapid evolvement. Figure 4 also shows ion vortexes on both sides of the jet, which are formed by the deflected ions from both the jet and ambient downstream plasma. These vortexes can also be observed in the downstream frame (see Figure S1 in Supporting Information S1), which is consistent with the observations by Plaschke and Hietala (2018); Plaschke et al. (2020).

4. Conclusions and Discussion

In this Letter, we present a 2-D hybrid simulation of the formation and evolution process of HSJ-driven bow waves. The simulated bow wave is characterized by the sharp enhancements in both magnetic field and ion

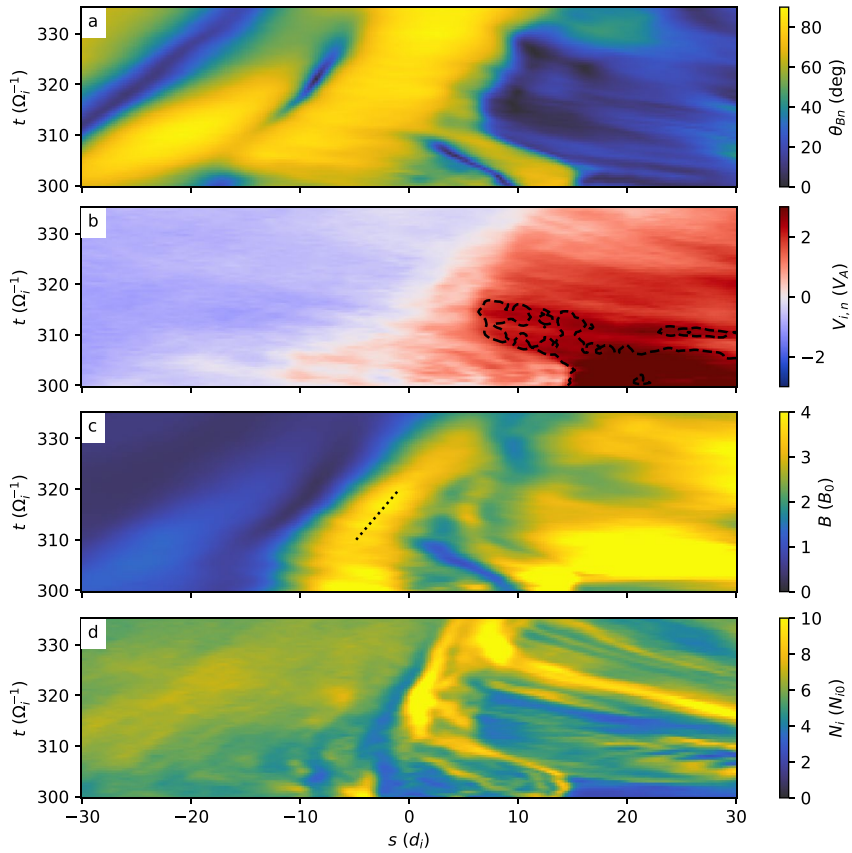

Figure 3. Time evolution of the line profile along BW1's normal direction (black dashed lines in Figure 2, purple dashed lines in the Movie S1) between $t = 300$ and 335 Ω_i^{-1}. (a) The angle between the magnetic field and the bow wave's normal direction θ_{Bn}, (b) ion velocity along BW1's normal direction in the bow wave frame $V_{i,n}$, (c) total magnetic field B, and (d) ion density N_i. The black dashed line in panel (b) shows the region where the relative velocity between the High-speed jet and the magnetic field structure on the bow wave's normal direction is super-magnetosonic. The dotted line in panel c shows the linear fitted path of the local peaks of the magnetic field.

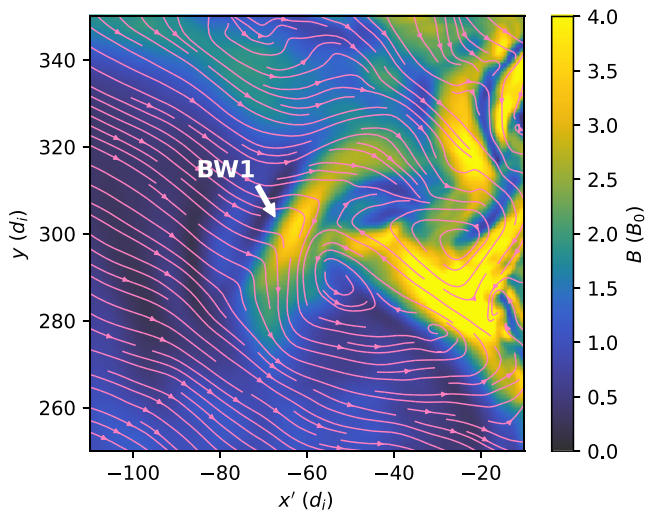

Figure 4. Ion flow in the bow wave frame at $t = 320$ Ω_i^{-1}. The color shows the total magnetic field, while the pink streamlines show the direction of the ion flow in the bow wave frame in the x-y plane (V_{ix}, V_{iy}).

density, with their peaks separated by the order of d_i. These properties are consistent with the previous satellite observations (Liu et al., 2019; Liu, Hietala, Angelopoulos, Omelchenko, et al., 2020). In our simulation, the bow wave is formed when the driving HSJ encounters a magnetic field structure, whose magnetic field is nearly perpendicular to the bulk velocity of the HSJ. During this process, the compression of the magnetic field leads to the sharp magnetic field enhancement on the downstream side of the bow wave, while the braking of the HSJ causes the pile up of ion density, resulting in the formation of a density peak on the jet side.

Our simulation shows that a bow wave is formed after a super-magnetosonic HSJ interacts with a distorted magnetic field structure, which can efficiently decelerate the ion flow of the HSJ when the angle between its magnetic field and the HSJ's bulk velocity is sufficiently large. The magnetic field structure leads to BW1 in our simulation is formed by shock-compressed foreshock waves transmitted downstream, but such structures can also originate from other shock processes, such as convected foreshock compressive structures (Suni et al., 2021), magnetic bundles formed by turbulent shock reformation (Omelchenko et al., 2021), or the curved magnetic field structures naturally formed during the evolution of HSJs (Guo et al., 2022). Raptis, Karlsson, Vaivads, Lindberg, et al. (2022) have reported an HSJ interacting with a

magnetic field structure, and the magnetic field direction of the structure is almost perpendicular to the bulk velocity of the HSJ, suggesting the possible formation of a bow wave ahead of the observed HSJ. As the HSJ drives the bow wave further downstream, it cannot continue to provide enough energy to sustain the bow wave due to its own deceleration (see Movie S1). This process can possibly convert HSJ's kinetic energy into thermal energy and contribute to magnetosheath heating (Liu et al., 2019; Liu, Hietala, Angelopoulos, Vainio, & Omelchenko, 2020), and play a role in forming the downstream ion distributions in a quasi-parallel shock.

Liu, Hietala, Angelopoulos, Omelchenko, et al. (2020) found that the ratio of the number of HSJs observed with a bow wave to those observed without one is higher close to the magnetopause than near the bow shock. In our simulation, however, the bow waves appear within ∼100 d_i downstream of the shock. This difference is mainly caused by the simplified shock geometry used in our simulation. In our simulation, the magnetopause is replaced by a reflecting wall on the left x boundary, and downstream plasma cannot flow around the magnetopause like in the real Earth's magnetosheath due to the periodic y boundaries. As a consequence, plasma is fully decelerated in the near downstream rather than at the magnetopause. Although the physical process of the bow wave's formation is still the same, direct comparison with the statistical result will require a 3D global simulation.

Data Availability Statement

The simulation data (Ren, 2023) used to plot the figures in this paper can be downloaded from "National Space Science Data Center, National Science & Technology Infrastructure of China".

Acknowledgments
This work was supported by NSFC Grant 42174181 and the Strategic Priority Research Program of Chinese Academy of Sciences Grant XDB41000000. Computer resources were provided by the Hefei Advanced Computing Center of China, and the data hosting service is provided by the "National Space Science Data Center, National Science & Technology Infrastructure of China (www.nssdc.ac.cn)."

References

Archer, M. O., & Horbury, T. S. (2013). Magnetosheath dynamic pressure enhancements: Occurrence and typical properties. *Annales Geophysicae*, *31*(2), 319–331. https://doi.org/10.5194/angeo-31-319-2013

Guo, J., Lu, S., Lu, Q., Lin, Y., Wang, X., Ren, J., et al. (2022). Large-scale high-speed jets in earth's magnetosheath: Global hybrid simulations. *Journal of Geophysical Research: Space Physics*, *127*(6), e30704. https://doi.org/10.1029/2022ja030477

Hao, Y., Lembege, B., Lu, Q., & Guo, F. (2016). Formation of downstream high-speed jets by a rippled nonstationary quasi-parallel shock: 2-D hybrid simulations. *Journal of Geophysical Research: Space Physics*, *121*(3), 2080–2094. https://doi.org/10.1002/2015ja021419

Hietala, H., Laitinen, T. V., Andréeová, K., Vainio, R., Vaivads, A., Palmroth, M., et al. (2009). Supermagnetosonic jets behind a collisionless quasiparallel shock. *Physical Review Letters*, *103*(24), 245001. https://doi.org/10.1103/physrevlett.103.245001

Hietala, H., Partamies, N., Laitinen, T. V., Clausen, L. B. N., Facskó, G., Vaivads, A., et al. (2012). Supermagnetosonic subsolar magnetosheath jets and their effects: From the solar wind to the ionospheric convection. *Annales Geophysicae*, *30*(1), 33–48. https://doi.org/10.5194/angeo-30-33-2012

Karimabadi, H., Roytershteyn, V., Vu, H. X., Omelchenko, Y. A., Scudder, J., Daughton, W., et al. (2014). The link between shocks, turbulence, and magnetic reconnection in collisionless plasmas. *Physics of Plasmas*, *21*(6), 062308. https://doi.org/10.1063/1.4882875

Karlsson, T., Kullen, A., Liljeblad, E., Brenning, N., Nilsson, H., Gunell, H., & Hamrin, M. (2015). On the origin of magnetosheath plasmoids and their relation to magnetosheath jets. *Journal of Geophysical Research: Space Physics*, *120*(9), 7390–7403. https://doi.org/10.1002/2015ja021487

Liu, T. Z., Hietala, H., Angelopoulos, V., Omelchenko, Y., Roytershteyn, V., & Vainio, R. (2019). THEMIS observations of particle acceleration by a magnetosheath jet-driven bow wave. *Geophysical Research Letters*, *46*(14), 7929–7936. https://doi.org/10.1029/2019gl082614

Liu, T. Z., Hietala, H., Angelopoulos, V., Omelchenko, Y., Vainio, R., & Plaschke, F. (2020). Statistical study of magnetosheath jet-driven bow waves. *Journal of Geophysical Research: Space Physics*, *125*(7), e2019JA027710. https://doi.org/10.1029/2019ja027710

Liu, T. Z., Hietala, H., Angelopoulos, V., Vainio, R., & Omelchenko, Y. (2020). Electron acceleration by magnetosheath jet-driven bow waves. *Journal of Geophysical Research: Space Physics*, *125*(7), e2019JA027709. https://doi.org/10.1029/2019ja027709

Lu, Q. M., Xia, L. D., & Wang, S. (2006). Hybrid simulations of parallel and oblique electromagnetic alpha/proton instabilities in the solar wind. *Journal of Geophysical Research*, *111*(A9), A09101. https://doi.org/10.1029/2006ja011752

Němeček, Z., Šafránková, J., Přech, L., Sibeck, D. G., Kokubun, S., & Mukai, T. (1998). Transient flux enhancements in the magnetosheath. *Geophysical Research Letters*, *25*(8), 1273–1276. https://doi.org/10.1029/98gl50873

Omelchenko, Y. A., Chen, L.-J., & Ng, J. (2021). 3D space-time adaptive hybrid simulations of magnetosheath high-speed jets. *Journal of Geophysical Research: Space Physics*, *126*(7), e2020JA029035. https://doi.org/10.1029/2020ja029035

Plaschke, F., Glassmeier, K.-H., Sibeck, D. G., Auster, H. U., Constantinescu, O. D., Angelopoulos, V., & Magnes, W. (2009). Magnetopause surface oscillation frequencies at different solar wind conditions. *Annales Geophysicae*, *27*(12), 4521–4532. https://doi.org/10.5194/angeo-27-4521-2009

Plaschke, F., & Hietala, H. (2018). Plasma flow patterns in and around magnetosheath jets. *Annales Geophysicae*, *36*(3), 695–703. https://doi.org/10.5194/angeo-36-695-2018

Plaschke, F., Hietala, H., & Angelopoulos, V. (2013). Anti-sunward high-speed jets in the subsolar magnetosheath. *Annales Geophysicae*, *31*(10), 1877–1889. https://doi.org/10.5194/angeo-31-1877-2013

Plaschke, F., Jernej, M., Hietala, H., & Vuorinen, L. (2020). On the alignment of velocity and magnetic fields within magnetosheath jets. *Annales Geophysicae*, *38*(2), 287–296. https://doi.org/10.5194/angeo-38-287-2020

Raptis, S., Karlsson, T., Vaivads, A., Lindberg, M., Johlander, A., & Trollvik, H. (2022). On magnetosheath jet kinetic structure and plasma properties. *Geophysical Research Letters*, *49*(21), A08217. https://doi.org/10.1029/2022gl100678

Raptis, S., Karlsson, T., Vaivads, A., Pollock, C., Plaschke, F., Johlander, A., et al. (2022). Downstream high-speed plasma jet generation as a direct consequence of shock reformation. *Nature Communications*, *13*(1), 598. https://doi.org/10.1038/s41467-022-28110-4

Ren, J. (2023). Data for "hybrid simulation of magnetosheath jet-driven bow waves" [Dataset]. Science Data Bank. https://doi.org/10.57760/SCIENCEDB.11230

Ren, J., Lu, Q., Guo, J., Gao, X., Lu, S., Wang, S., & Wang, R. (2023). Two-dimensional hybrid simulations of high-speed jets downstream of quasi-parallel shocks. *Journal of Geophysical Research: Space Physics*, *128*(8), e2021JA029571. https://doi.org/10.1029/2023ja031699

Suni, J., Palmroth, M., Turc, L., Battarbee, M., Johlander, A., Tarvus, V., et al. (2021). Connection between foreshock structures and the generation of magnetosheath jets: Vlasiator results. *Geophysical Research Letters*, *48*(20), e2021GL095655. https://doi.org/10.1029/2021gl095655

Vuorinen, L., Vainio, R., Hietala, H., & Liu, T. Z. (2022). Monte Carlo simulations of electron acceleration at bow waves driven by fast jets in the earth's magnetosheath. *The Astrophysical Journal*, *934*(2), 165. https://doi.org/10.3847/1538-4357/ac7f42

Wang, B., Nishimura, Y., Hietala, H., Shen, X.-C., Shi, Q., Zhang, H., et al. (2018). Dayside magnetospheric and ionospheric responses to a foreshock transient on 25 June 2008: 2. 2-D evolution based on dayside auroral imaging. *Journal of Geophysical Research: Space Physics*, *123*(8), 6347–6359. https://doi.org/10.1029/2017ja024846